ADVANCED MATERIALS

www.advmat.de

High-Brightness Blue and White LEDs based on Inorganic Perovskite Nanocrystals and their Composites

*En-Ping Yao, Zhanlue Yang, Lei Meng, Pengyu Sun, Shiqi Dong, Ye Yang, and Yang Yang**

Inorganic metal halide perovskite nanocrystals (NCs) have been employed universally in light-emitting applications during the past two years. Here, blue-emission (≈470 nm) Cs-based perovskite NCs are derived by directly mixing synthesized bromide and chloride nanocrystals with a weight ratio of 2:1. High-brightness blue perovskite light-emitting diodes (PeLEDs) are obtained by controlling the grain size of the perovskite films. Moreover, a white PeLED is demonstrated for the first time by blending orange polymer materials with the blue perovskite nanocrystals as the active layer. Exciton transfer from the blue nanocrystals to the orange polymers via Förster or Dexter energy transfer is analyzed through time resolved photoluminescence. By tuning the ratio between the perovskite nanocrystals and polymers, pure white light is achieved with the a CIE coordinate at (0.33,0.34).

Metal-halide-based perovskites have attracted much attention in recent years due to their excellent performance for semiconducting applications.[1–9] The perovskite structure can be simply constructed into a polycrystalline thin film through a solution process without high-temperature treatment, which has high potential in applying to large areas and flexible substrates. Their strong photoluminescent properties and the tunable bandgap of the polycrystalline material, along with the narrow full width at half maximum (FWHM) of the luminescence spectra, give them high potential for the use in light-emitting diodes (LEDs).[10–13] The organometal halide perovskite light emitting diodes (PeLEDs) have displayed a current efficiency of over 42.9 cd A^{-1} on green-light emission by minimizing the grain sizes of perovskite film using the nanocrystal pinning (NCP) method, showing high possibilities for integration into lighting devices.[13] Recently, all-inorganic perovskite, $CsPbX_3$ (X represents a halogen) nanocrystals (NCs) synthesized by solution-phase chemistry approach have been recently reported by several groups,[14–18] exhibiting superior thermal stability and high photoluminescence (PL) quantum yield (QY) reaching 90% in solution.[14] The outstanding properties of $CsPbX_3$ NCs make them especially attractive for electroluminescence (EL) applications, with more and more groups[19–25] investigating LEDs using $CsPbX_3$ NCs, since the first work was reported by Song et al.[19]

However, blue PeLEDs are still under investigation and will play an important role in display applications. Li et al. reported Cs-based blue PeLEDs with an emission peak at 480 nm and a brightness at 8.7 cd m^{-2}.[22] Song et al. have also reported bright blue $CsPbX_3$ PeLEDs with maximum luminance of 742 cd m^{-2} centered at 455 nm. Another brighter Cs-based blue PeLED was reported with maximum brightness of 35 cd m^{-2} and an emission peak at 490 nm.[24] In this work, we demonstrate a high brightness of blue all-inorganic PeLEDs with narrow FWHM of the PL and EL spectra by controlling the dispersity of $CsPbBr_xCl_{3-x}$ nanocrystals in the deposition solution to determine the grain size of perovskite films. Different mixed-phase $CsPbBr_xCl_{3-x}$ nanocrystals can be simply derived through blending the pure $CsPbBr_3$ and $CsPbCl_3$ nanocrystals dispersed in appropriate solvents according to the ligands around the nanocrystals. The mixed phases interestingly deliver narrow emission peak as reported by several groups.[26–29] Although pure $CsPbCl_3$ exhibits only 1% on PLQY, pure $CsPbBr_3$ can reach as high as 78% indicating that the tunable bandgap raises possibilities of a compromise between emission wavelength and luminescence efficiency. Since the emission wavelength can be modulated from pure $CsPbBr_3$, 510 nm, to pure $CsPbCl_3$, 390 nm, a blue emission of $CsPbBr_xCl_{3-x}$ nanoparticles was successfully obtained (≈470 nm) here. To reasonably choose the carrier types in the design of the device structure, ultraviolet photoelectron spectroscopy (UPS) was employed to characterize the conduction-band minimum (CBM) and the valence-band maximum (VBM) of the mixed phase $CsPbBr_xCl_{3-x}$. An important issue is that the solvents used to deposit the perovskite films not only determine the dispersity of the $CsPbBr_xCl_{3-x}$ nanocrystals in solution but also determine the grain sizes. By applying the appropriate solvent, the grain sizes of perovskite crystals can be controlled to be very tiny. Hence, we attribute the high-brightness blue PeLEDs to a benign quantum-confinement effect, in accordance with the small grain sizes of $CsPbBr_xCl_{3-x}$ films. With the bright blue EL, we can build the first white PeLEDs by blending with organic orange-light-emissive materials.

Although the mixing phenomena of $CsPbBr_3$ and $CsPbCl_3$ has been reported by several groups, some of which have even

Dr. E.-P. Yao, Z. Yang, L. Meng, P. Sun, S. Dong, Prof. Y. Yang
Department of Materials Science and Engineering
University of California, Los Angeles
Los Angeles, CA 90095, USA
E-mail: yangy@ucla.edu
Dr. E.-P. Yao
Advanced Optoelectronic Technology Center
National Cheng Kung University
Tainan 70101, Taiwan
Dr. Y. Yang
Chemistry and Nanoscience Science Center
National Renewable Energy Laboratory
Golden, CO 80401, USA

DOI: 10.1002/adma.201606859

 © 2017 WILEY-VCH Verlag GmbH & Co. KGaA, Weinheim

Pursuant to the DOE Public Access Plan, this document represents the authors' peer-reviewed, accepted manuscript. The published version of the article is available from the relevant publisher.

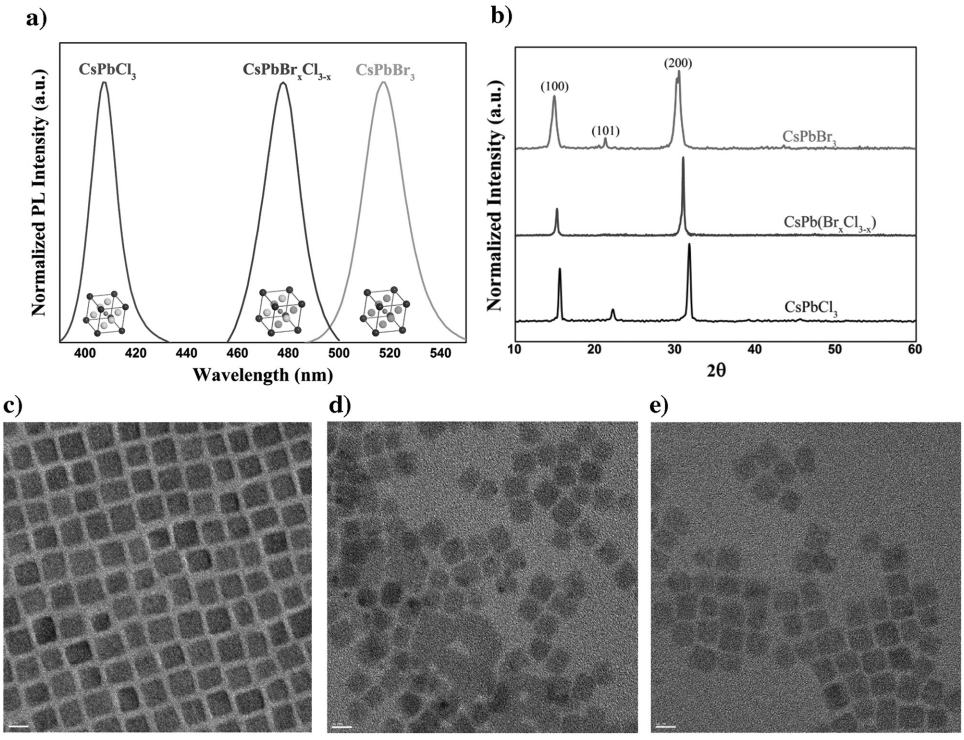

Figure 1. a,b) PL spectra (a) and XRD analysis (b) of $CsPbBr_3$, $CsPbCl_3$, and $CsPbBr_xCl_{3-x}$ nanocrystals. c–e) TEM images of $CsPbBr_3$ (c), $CsPbCl_3$ (d), and $CsPbBr_xCl_{3-x}$ (e) nanocrystals with the scale bars at nm.

fabricated perovskite LED devices taking advantage of the adjustable bandgap through mixing, the influence of mixing on both particle and film morphology has not yet been well studied. Perovskite materials are known for their structural sensitivity to external conditions, where phase transitions, structural distortion, and even degradation may occur.[30–33] Therefore, it is reasonable to investigate the possible effects induced by mixing of $CsPbBr_3$ and $CsPbCl_3$ perovskite materials, especially in terms of their influence on film morphology, which essentially determines the performance of LED devices.

Figure 1a shows the PL spectra of $CsPbBr_3$, $CsPbCl_3$, and their solution mixture with the peak values at 390, 510, and 470 nm, respectively. The three different spectra indicate that the $CsPbBr_3$ and $CsPbCl_3$ nanocrystals were well mixed into a new phase, $CsPbBr_xCl_{3-x}$, with the emission peak between them. The new phase exhibited a unique optical bandgap at 2.64 eV with very narrow FWHM, similar to $CsPbBr_3$ and $CsPbCl_3$ nanocrystals. The X-ray photoelectron spectroscopy (XPS) analysis on the film deposited with $CsPbBr_xCl_{3-x}$ solution (Figure S1, Supporting Information) shows that both Br and Cl exist in the film consisting of Cs and Pb as well. The new phase of $CsPbBr_xCl_{3-x}$ should lead to another new crystalline structure as the crystal units inserted with each PL spectrum in Figure 1a. Figure 1b shows the X-ray diffraction (XRD) spectrum for $CsPbBr_3$, $CsPbCl_3$, and $CsPbBr_xCl_{3-x}$ spin coated onto indium tin oxide (ITO) glass. As can be seen, with an increasing amount of Br in $CsPbCl_3$, the diffraction peaks gradually move to low-angle positions. Further considering the single-peak photoluminescence of $CsPbBr_xCl_{3-x}$, it is highly possible that mixing of $CsPbBr_3$ and $CsPbCl_3$ will form a solid solution, where Br^- is partially replaced by Cl^-. Despite the peak shift, all of the three perovskite thin films show a texture feature, where the high intensity peaks of (100), compared to that of (101), clearly shows a preferred orientation. Moreover, after the mixing of $CsPbBr_3$ and $CsPbCl_3$, the (101) peak even disappeared. This indicates a much better out-plane texture of $CsPbBr_xCl_{3-x}$ thin film, although its in-plane alignment is slightly worse than that of $CsPbBr_3$, indicated by scanning electron microscopy (SEM) and transmission electron microscopy (TEM) images.

Since the new phase is simply derived by blending $CsPbBr_3$ and $CsPbCl_3$ together, it would be interesting to study the crystal size and crystallinity. The comparison of the TEM images of $CsPbBr_3$, $CsPbCl_3$, and $CsPbBr_xCl_{3-x}$ nanocrystals is shown in Figure 1c,d,e, respectively. $CsPbBr_3$, $CsPbCl_3$, and $CsPbBr_xCl_{3-x}$ all exhibited similar particle sizes and shapes, indicating that the mixing behavior merely changed the particle morphology. Although mixing of $CsPbBr_3$ and $CsPbCl_3$ has a minor influence on particle size, it further determines the aggregation behavior of the nanoparticles. While $CsPbBr_3$ nanoparticles exhibit perfect orderly alignment, $CsPbCl_3$ nanoparticles are poorly aligned and even tend to aggregate. As for $CsPbBr_xCl_{3-x}$, although no sign of aggregation is identified, the alignment is still worse than that of $CsPbBr_3$ nanoparticles.

The essential reason for the different order in the TEM images between $CsPbBr_3$ and $CsPbCl_3$ nanocrystals lies with the ligands. Oleylamine is believed to be the ligand that modifies the perovskite nanocrystals in our reaction system. The nucleophilic nature of oleylamine enables its combination to the cations in $CsPbBr_xCl_{3-x}$, forming ligand-modified

© 2017 WILEY-VCH Verlag GmbH & Co. KGaA, Weinheim

Pursuant to the DOE Public Access Plan, this document represents the authors' peer-reviewed, accepted manuscript. The published version of the article is available from the relevant publisher.

perovskite nanocrystals. However, the combination strength of oleylamine ligand with cations is heavily determined by the surrounding anions, either Cl^- or Br^-. Considering that the electronegativity of Cl^- (3.0) is higher than that of Br^- (2.8), combination between Cl^- and a cation is much stronger, further weakening the combination between the ligand and the perovskite nanocrystals. The difference in the ligand-modification situation between the $CsPbBr_3$ and $CsPbCl_3$ solutions explains their difference in dispersity, and also explains their mixture $CsPbBr_xCl_{3-x}$ having intermediate dispersity.

Since the perovskite nanocrystals are surrounded with nonpolar organic ligands, they can be simply dispersed in some nonpolar organic solvents, such as toluene and hexane. From the point of view of polarity, hexane (0.1) is much lower than toluene (2.4), and the dispersity of perovskite nanocrystals in hexane is much better than in toluene due to the polarity of the oleylamine ligands. However, the boiling point of hexane (68 °C) is lower than that of toluene (110.6 °C), and for solution processes, when the boiling point of the solvent is too low, the concentration of the solution will vary significantly during the exposure under atmospheric conditions at room temperature. Therefore, dispersing the nanocrystals with toluene for the spin-coating process is more suitable for reproducibility. In order to improve the dispersity of the $CsPbBr_xCl_{3-x}$ nanocrystals solution, we blended hexane with toluene at the volume ratio of 0% (solvent A), 50% (solvent B), and 90% (solvent C) as the solvent for the deposition of the $CsPbBr_xCl_{3-x}$ nanocrystal film. The difference in dispersity leads to different aggregation of the $CsPbBr_xCl_{3-x}$ nanocrystals in the solution, which can be derived using dynamic light scattering (DLS). The aggregation property, which can be defined as the particle size in solvent, of the $CsPbBr_xCl_{3-x}$ nanocrystals in solvent A, solvent B, and solvent C is 500, 350, and 300 nm, respectively, (Figure S2, Supporting Information). This result indicates that a better dispersity of nanocrystals was obtained by mixing hexane with toluene. With different aggregation properties, the aggregation process of the $CsPbBr_xCl_{3-x}$ nanocrystals while depositing the films would be different as well. **Figure 2**a–c show SEM images of the $CsPbBr_xCl_{3-x}$ nanocrystal film deposited with solvent in different ratios of toluene to hexane, respectively. The films show uniform small $CsPbBr_xCl_{3-x}$ grains without any pinholes, indicating that the $CsPbBr_xCl_{3-x}$ nanocrystals are binding together and completely cover the hole-transport layer. By depositing with different solvents, the grain size decreases obviously with a higher ratio of hexane in the solution. The PL intensity of the films deposited via solvent A, B, and C (Figure S3, Supporting Information) indicates that the smaller grain size of perovskite film leads to better quantum confinement and high PL intensity, similar to the result of the grain-size control from the NCP process reported by Cho et al. The result implies that the better dispersity of the $CsPbBr_xCl_{3-x}$ nanocrystals in the solvent leads to a smaller grain size without changing the coverage of the film. The smoother surface can also be obtained by blending a higher ratio of hexane with

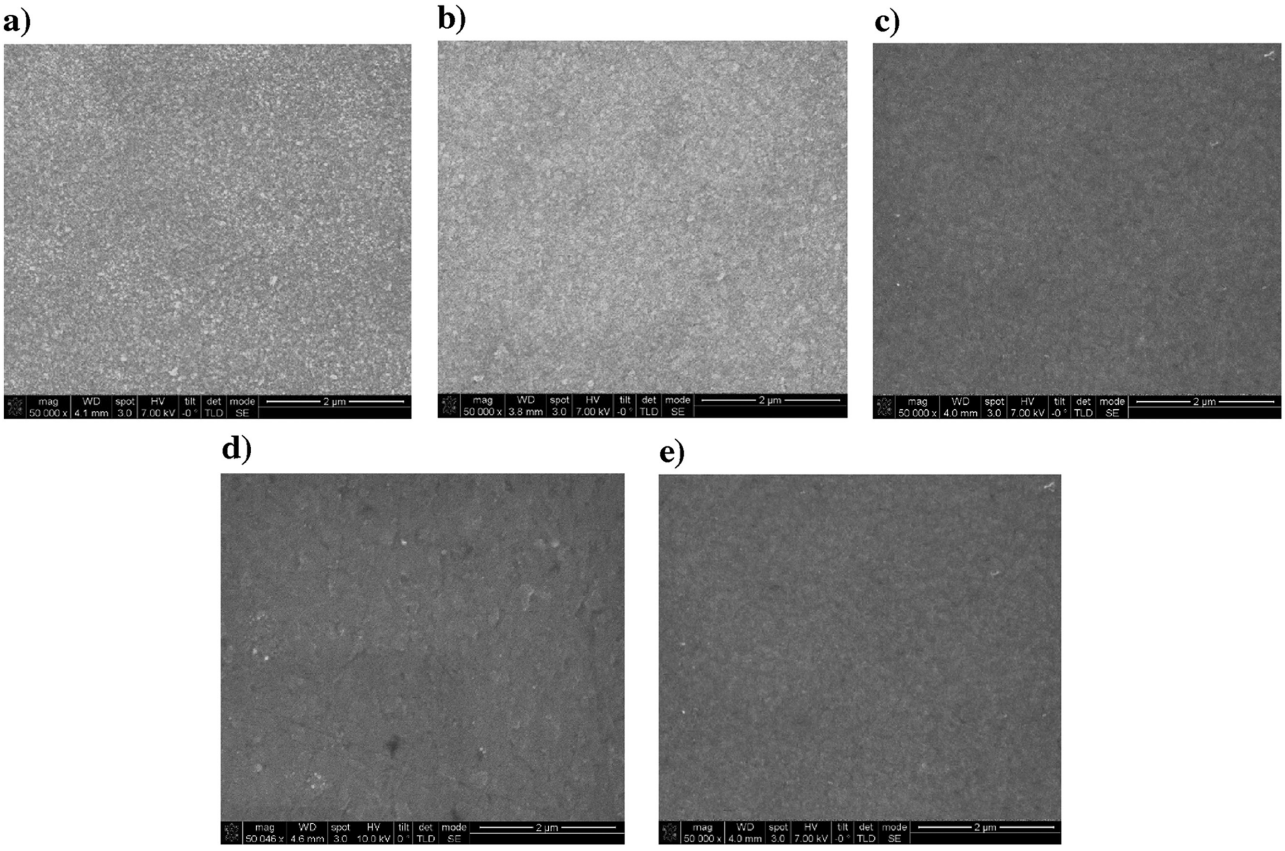

Figure 2. SEM images of $CsPbBr_xCl_{3-x}$ films deposited with solvent in toluene:hexane ratio of: a) 1:0, b) 1:1, c) 1:3, d) 1:5, and e) 1:9.

© 2017 WILEY-VCH Verlag GmbH & Co. KGaA, Weinheim

Pursuant to the DOE Public Access Plan, this document represents the authors' peer-reviewed, accepted manuscript. The published version of the article is available from the relevant publisher.

toluene as the solvent since the smaller grains stack more compactly and with better dispersity in the nanocrystal solution. Controlling the film morphology of the perovskite layer is a critical factor in the device performance.

In order to achieve blue PeLEDs, the CBM and the VBM of $CsPbBr_xCl_{3-x}$ are required for the design of carrier-injection/blocking layers between the perovskite layer. The optical bandgap of $CsPbBr_xCl_{3-x}$ was derived directly from the PL peak presented in Figure 1a, and the CBM and VBM are defined through optical bandgap and UPS measurements (Figure S4, Supporting Information) at 2.83 and 5.5 eV, respectively. The PeLED was built up as the structure shown in **Figure 3**a with the energy-band diagram of each layer illustrated. By utilizing nickel oxide (NiO_x) as the hole-transport layer, not only does its thermal and chemical stability simplify the deposition process of the perovskite layer, but its wide bandgap also efficiently blocks the electron transport from the perovskite layer to the anode as the energy barrier shown in Figure 3a. The commonly used electron-transport and hole-blocking material, 2,2′,2″(1,3,5-benzinetriyl)-tris(1-phenyl-1-H-benzimidazole) (TPBi), was directly deposited on the perovskite layer to prevent the leakage of holes from the perovskite layer to the cathode as the energy barrier shown in Figure 3a. The sandwich structure would successfully confine the holes and electrons inside the perovskite layer and increase the probability of the recombination of opposite charge carriers.

Figure 3b shows the current-density–luminescence–voltage (*J–L–V*) curve of PeLEDs with the perovskite films deposited with solvent A, B, and C. It shows that the film deposited with a large proportion of hexane yields higher luminescence indicating that the perovskite film with smaller grain size has a benign quantum-confinement effect; a result observed in the work proposed by Cho et al.[13] Moreover, the perovskite film with the smoother surface morphology, caused by depositing with a larger proportion of hexane, results in a lower trap density and better carrier-injection property at the interface between $CsPbBr_xCl_{3-x}$ and TPBi with lower turn-on voltage on the PeLED. The brightest device, processed with solvent C, reached 350 cd m^{-2}, which is the brightest blue PeLED so far. The best current efficiency of the brightest device achieved 0.18 cd A^{-1} with the EQE at 0.07%. The electroluminescence spectrum of the device with solvent C driving at 5 V is depicted in Figure 3c, showing a similar peak in the PL spectrum at 470 nm and extremely narrow FWHM around 20 nm, with a photo of the working device as the inset. In addition, there is nearly no difference in the peak value of the EL spectra of the PeLED under different driving voltages, as shown in Figure S6a in the Supporting Information; however, the redshift still happened while driving the device for a period of time in the EL spectra, depicted in Figure S6b in the Supporting Information, due to phase segregation into purer halide phases as the same phenomenon reported by Li et al.[22] With the bright blue PeLED, there is great potential to achieve multiple colors by integrating with green and red LEDs.

Here, we demonstrate a white LED by blending an orange polymeric material, poly[2-methoxy-5-(2-ethylhexyloxy)-1,4-phenylenevinylene] (MEH:PPV), with $CsPbBr_xCl_{3-x}$ nanocrystals as the active layer, using a similar device structure to the blue PeLEDs demonstrated in **Figure 4**a. The different weight ratios

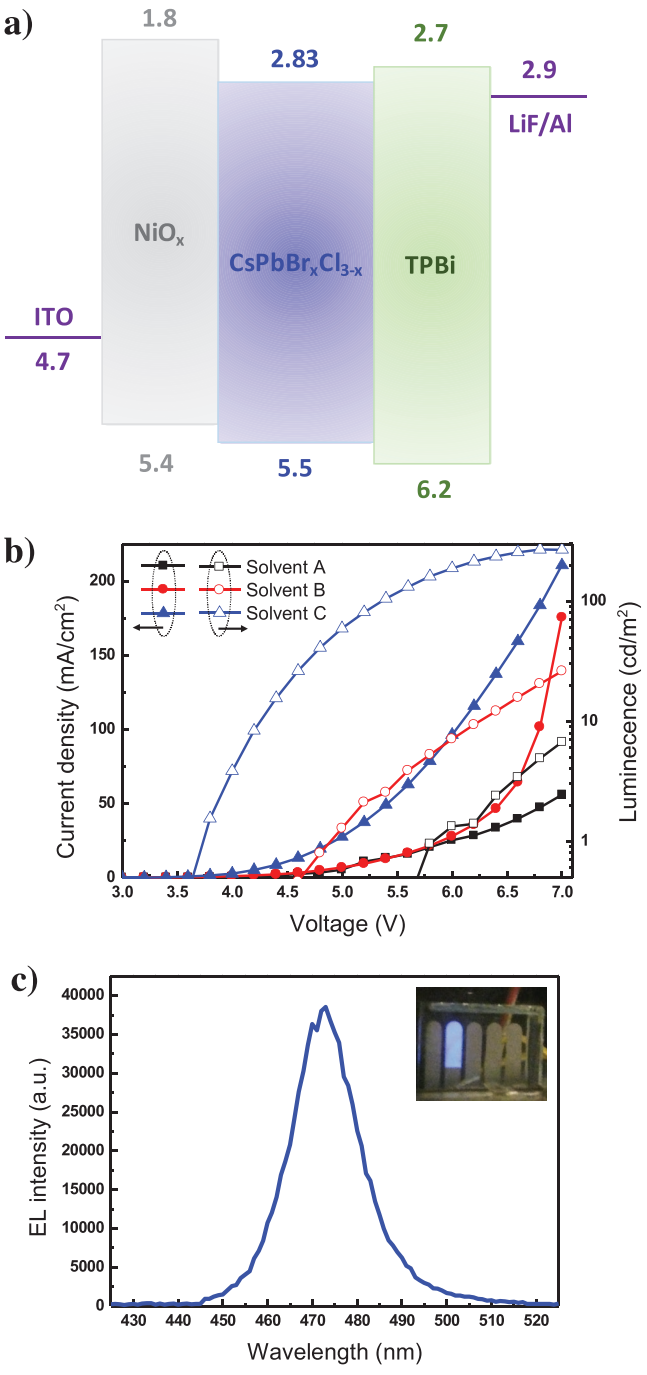

Figure 3. a) Schematic band structure of $CsPbBr_xCl_{3-x}$ nanocrystal-based blue LED. b) *J–L–V* curves of $CsPbBr_xCl_{3-x}$ nanocrystal-based blue LED deposited with solvent A, solvent B, and solvent C. c) The EL spectrum of $CsPbBr_xCl_{3-x}$ nanocrystal-based blue LED.

of $CsPbBr_xCl_{3-x}$ to MEH:PPV were employed as the active layer of the LEDs at ratios of 1:0, 18:1, 9:1, 3:1, and 0:1. By confining the electrons and holes in $CsPbBr_xCl_{3-x}$ and MEH:PPV with radiative combination, both the materials emit the light depicted in the EL spectra in Figure 4b. The EL spectra show two PL peaks at 470 nm, with a narrow FWHM, and 560 nm, with broad FWHM, corresponding to $CsPbBr_xCl_{3-x}$ and MEH:PPV,

© 2017 WILEY-VCH Verlag GmbH & Co. KGaA, Weinheim

Pursuant to the DOE Public Access Plan, this document represents the authors' peer-reviewed, accepted manuscript. The published version of the article is available from the relevant publisher.

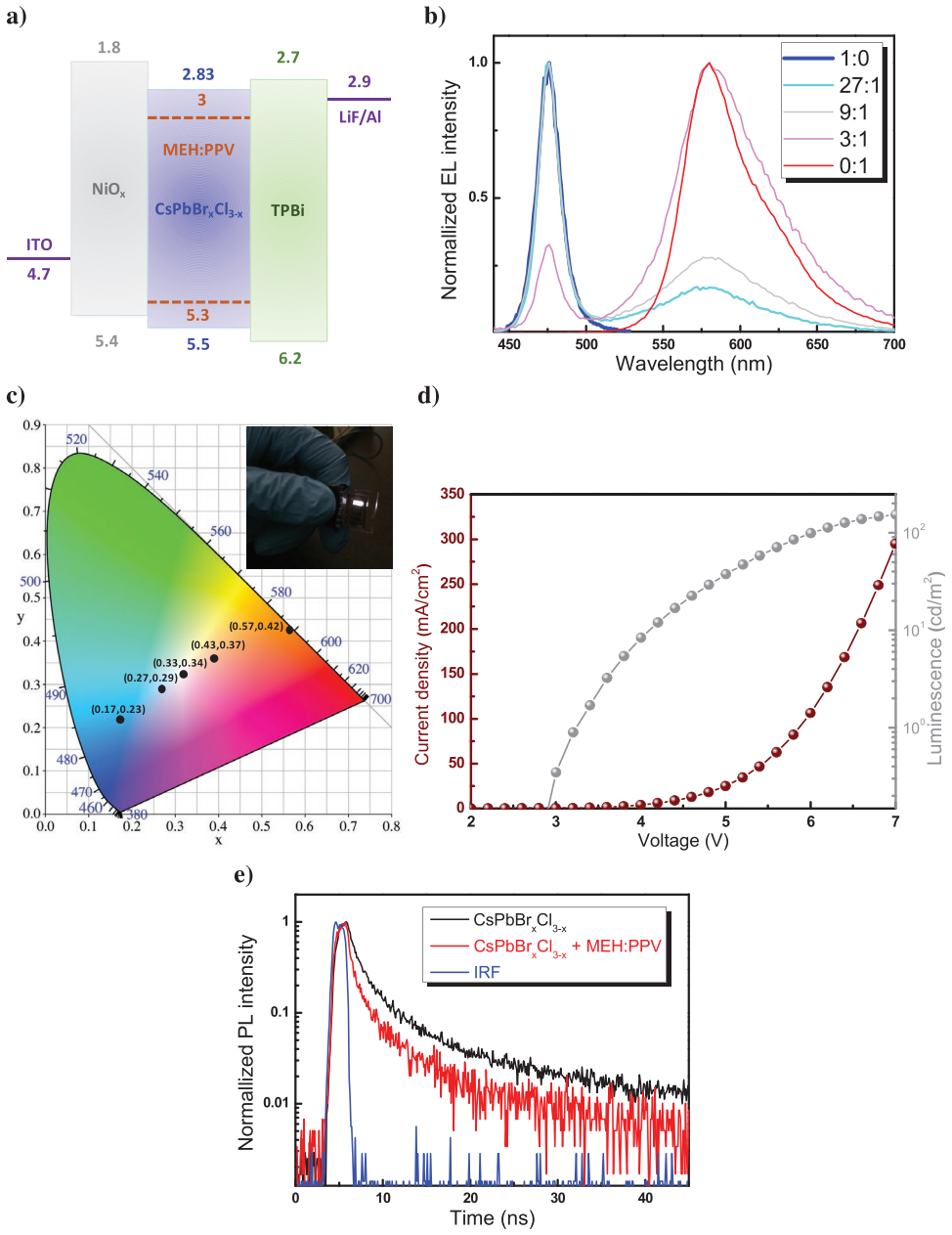

Figure 4. a) Schematic band structure, b) EL spectra, c) CIE coordinate, and d) *J–L–V* curve, of $CsPbBr_xCl_{3-x}$ nanocrystal and MEH:PPV blend white LED. e) TRPL of $CsPbBr_xCl_{3-x}$ nanocrystals blending with and without MEH:PPV films.

respectively. The increase of the MEH:PPV weight ratio led to higher EL intensity ratio of MEH:PPV than the EL intensity of $CsPbBr_xCl_{3-x}$. The Commission Internationale de l'Eclairage (CIE) chromaticity coordinate of the LEDs with different weight ratios of $CsPbBr_xCl_{3-x}$ to MEH:PPV are depicted in Figure 4c. When the weight ratio was 9:1, the ultimate light emitted out while driving under 8 V shows white light, as in the photo presented in the inset of Figure 4c, with its CIE chromaticity coordinate at (0.33, 0.34), and with the *J–L–V* curve depicted in Figure 4d.

In the study of organic LEDs, when blending two or more emissive materials as the light-emission layer, the excitons tend to transition from high-bandgap materials to lower-bandgap materials via Förster or Dexter transfer quenching process. In this system, the $CsPbBr_xCl_{3-x}$ corresponds to the high-bandgap material and the MEH:PPV corresponds to the low-bandgap material. The lowest unoccupied molecular orbital (LUMO) and the highest occupied molecular orbital (HOMO) of MEH:PPV are sandwiched by the CBM and VBM of $CsPbBr_xCl_{3-x}$. Therefore, the excitons in $CsPbBr_xCl_{3-x}$ would easily transfer to MEH:PPV via a Dexter energy-transfer mechanism. Förster energy transfer can happen simultaneously due to the emission range of $CsPbBr_xCl_{3-x}$, which is fully covered by the absorption range of MEH:PPV (Figure S5, Supporting Information). To verify whether the excitons transfer from $CsPbBr_xCl_{3-x}$ to MEH:PPV, time-resolved PL of the films with and without

© 2017 WILEY-VCH Verlag GmbH & Co. KGaA, Weinheim

Pursuant to the DOE Public Access Plan, this document represents the authors' peer-reviewed, accepted manuscript. The published version of the article is available from the relevant publisher.

blending of MEH:PPV into $CsPbBr_xCl_{3-x}$ nanocrystals was measured to investigate the quenching effect as shown in Figure 4e. The result shows that the PL lifetime decreased by blending the MEH:PPV with $CsPbBr_xCl_{3-x}$, indicating that the excitons were quenching from $CsPbBr_xCl_{3-x}$ to MEH:PPV. By transferring the excitons from $CsPbBr_xCl_{3-x}$ to MEH:PPV, the weight proportion of MEH:PPV does not need to be equal to $CsPbBr_xCl_{3-x}$ to produce a comparable intensity of orange light to achieve white-light-emitting devices. This work indicates that the perovskite nanocrystals can directly work with organic materials as the light-emission layer, and composite light can be simply modulated to pure white light not only by tuning the ratio between the perovskite nanocrystals and the organic materials, but also by varying the ratio of halogens in the perovskite nanocrystals.

In this work, the $CsPbBr_xCl_{3-x}$ nanocrystals were synthesized to achieve blue emission with a peak at 470 nm and with narrow bandwidth. The particle sizes of the nanocrystals in the light-emission layer were controlled to around 15 nm, leading to a better quantum-confinement effect. By designing the preferred device structure, the brightness reached 350 cd m^{-2}. Based on the high-brightness blue PeLEDs, the white LED can be derived by directly integrating MEH:PPV into the active layer with the CIE chromaticity coordinate at (0.33,0.34). The purity of the white LED can be tuned not only by the ratio between two different emissive materials but also by changing the ratio between the halogen in the perovskite crystals, demonstrating its high potential in applications such as lighting devices and displays in the future.

Experimental Section

Nanocrystals Synthesis: $CsPbBr_xCl_{3-x}$ was synthesized with reference to a previously reported method.[14] Cs_2CO_3 (0.407 g, Aldrich, 99.995%), octadecene (20 mL, ODE, Sigma–Aldrich, 90%), and oleic acid (1.25 mL, OA, Sigma–Aldrich, 90%) were loaded into a 50 mL three-neck flask, and subsequently dried for 2 h at 150 °C in Ar. Cs-oleate with yellow color was then obtained. ODE (100 mL), oleylamine (12.5 mL, OLA, Sigma–Aldrich, 70%), 12.5 mL OA and PbX_2 (3.76 mmol) such as $PbBr_2$ (1.38 g, Sigma–Aldrich, 99.999%), and $PbCl_2$ (1.04 g, Sigma–Aldrich, 99.999%) were loaded into a 500 mL three-neck flask and dried under vacuum for 2 h at 120 °C. After that, the temperature was raised to 170 °C for $CsPbBr_3$ and 200 °C for $CsPbCl_3$, and then 12 mL of 0.125 M Cs-oleate solution were injected within 5 s. Allowing for 1 min reaction, the mixture was immediately cooled by way of an ice-water bath. For $CsPbCl_3$, 25 mL of trioctylphosphine were further added into the reaction system. After the ice-water cooling, nanocrystals were precipitated out by adding tert-butanol (Fisher Chemical, Certified) as an antisolvent, followed by centrifugation at 8000 rpm for 8 min. After discarding the supernatant, the as-obtained particles were redispersed in hexane (EMD, 95%) and were filtered through 0.2 µm syringes. Tert-BuOH was used for the second time to precipitate the nanocrystals, followed by centrifugation. The obtained nanocrystals were dispersed in toluene or toluene/hexane joint solvent for application later.

NiO_x Precursor Solution: Nickel(II) nitrate hexahydrate ($Ni(NO_3)_2{\cdot}6H_2O$) (Sigma–Aldrich) was dissolved in an ethylene glycol solution containing 1 M nickel(II) nitrate hexahydrate with ethylenediamine (Aldrich).

Device Fabrication and Characterization: PeLEDs were fabricated on ITO-coated glass substrates, which served as the anode. The ITO substrates were ultrasonically cleaned in detergent, deionized water, acetone, and isopropyl alcohol. The NiO_x precursor was spin coated on the ITO and annealed at 300 °C for 60 min in ambient air. The $CsPbBr_xCl_{3-x}$ nanocrystals in solvent A, solvent B, and solvent C (5 mg mL^{-1}) were spin coated on the NiO_x layers and annealed at 90 °C for 3 min in ambient air. The white-emission layers were deposited from the solution, with different weight-ratio compositions between $CsPbBr_xCl_{3-x}$ and MEH:PPV. The perovskite-coated samples were then transferred into a vacuum chamber for the thermal vapor deposition of TPBi, LiF, and Al at rates of 0.1, 0.1, and 0.2 nm s^{-1}, respectively. The device area was 0.1 cm^2, defined by the overlapping section between the pattern of ITO and the electrode from the shadow mask. The *J–L–V* characteristics of PeLEDs were measured using two Keithley 2400 source units. The intensity of the EL was recorded by a silicon photodiode (Hamamatsu S1133-14, Japan) as calibrated by a PR650 spectrophotometer (Photo Research, USA).

Physical and Chemical Analysis: The sizes of the as-synthesized nanocrystals were characterized using Titan S/TEM with 300 kV electron-beam energy. Samples for TEM were prepared on a 300 mesh copper grid coated with an ultrathin carbon supporting film. A field-emission SEM (FEI Nova 230 NanoSEM) was used to acquire the SEM images. The instrument used an electron beam accelerated at 7 kV, enabling operation at a variety of currents. XRD patterns (θ–2θ scans) were obtained from samples of perovskite deposited on substrates using a double-axis X-ray diffractometer (Bruker D8) equipped with a focusing-graded X-ray mirror with monochromatic Cu Kα (λ = 1.5405 Å) radiation source. Scans were taken with a 0.5 mm wide source and detector slits, and with X-ray generator settings of 40 kV and 30 mA. PL was measured using a Horiba–Jobin–Yvon system with excitation at 600 nm. The PL photons were counted by a Picoharp 300 after being preamplified by a preamplifier module (PAM102, PicoQuant). EL spectra were taken using the same spectrometer as PL with the devices driven at a constant current using a Keithley 2400 source unit. UPS measurements were carried out to determine the work function of the materials, and a He discharge lamp, emitting ultraviolet energy at 21.2 eV, was used for excitation. All the UPS measurements of the onset of the photoemission to determine the work function were performed using standard procedures with a −9 V bias applied to the samples. Beckman Coulter N4 Plus was used for DLS measurement. The DLS measurements were taken under 20 °C temperature with 90° detector angle, and 10 mW helium–neon 632.8 nm incident laser. DLS data was further processed using the PCS Control software. Samples were diluted to the same concentration in corresponding toluene/hexane solvents, and the intensity of all solutions was within 10^5 to 10^6.

Supporting Information

Supporting Information is available from the Wiley Online Library or from the author.

Acknowledgements

E.-P.Y. and Z.Y. contributed equally to this work. This work was financially supported by grants from the Air Force Office of Scientific Research (Grant number FA9550-15-1-0333, Program Manager: Dr. Charles Lee) and the National Science Foundation (Grant No. ECCS-1509955, Program Director: Dr. Nadia El-Masry and ECCS-1202231, Program Director: Dr. Radhakishan Baheti). The manuscript was proofread by Isaac Wang and Philip Li. E.-P.Y. and Ya.Y. designed the experiments. E.-P.Y. performed the devices fabrication and data analysis. Z.Y. synthesized all the nanocrystals and carried out the SEM, TEM, DLS, and XRD measurements. L.M. carried out the XPS and UPS measurements. P.S. conducted the PL and EL measurements. S.D. helped set up *J–L–V* measurement equipment. Ye Yang did the TRPL analysis. All the authors discussed the results and commented on the manuscript. Yang Yang planned and supervised the project.

© 2017 WILEY-VCH Verlag GmbH & Co. KGaA, Weinheim

Pursuant to the DOE Public Access Plan, this document represents the authors' peer-reviewed, accepted manuscript. The published version of the article is available from the relevant publisher.

Keywords

light-emitting diodes, nanocrystals, perovskites, white light

Received: December 19, 2016
Revised: February 13, 2017
Published online:

[1] A. Kojima, K. Teshima, Y. Shirai, T. Miyasaka, *J. Am. Chem. Soc.* **2009**, *131*, 6050.
[2] S. Kazim, M. K. Nazeeruddin, M. Grätzel, S. Ahmad, *Angew. Chem., Int. Ed.* **2014**, *53*, 2812.
[3] H. J. Snaith, *J. Phys. Chem. Lett.* **2013**, *4*, 3623.
[4] N. G. Park, *J. Phys. Chem. Lett.* **2013**, *4*, 2423.
[5] V. A. Online, P. Gao, M. K. Nazeeruddin, *Energy Environ. Sci.* **2014**, *1*, 2448.
[6] H. Zhou, Q. Chen, G. Li, S. Luo, T. Song, H.-S. Duan, Z. Hong, J. You, Y. Liu, Y. Yang, *Science* **2014**, *345*, 542.
[7] M. Green, T. Bein, *Nat. Mater.* **2015**, *14*, 559.
[8] W. S. Yang, J. H. Noh, N. J. Jeon, Y. C. Kim, S. Ryu, J. Seo, S. Il Seok, *Science* **2015**, *348*, 9272.
[9] N. Ahn, D. Y. Son, I. H. Jang, S. M. Kang, M. Choi, N. G. Park, *J. Am. Chem. Soc.* **2015**, *137*, 8696.
[10] J. Wang, N. Wang, Y. Jin, J. Si, Z. K. Tan, H. Du, L. Cheng, X. Dai, S. Bai, H. He, Z. Ye, M. L. Lai, R. H. Friend, W. Huang, *Adv. Mater.* **2015**, *27*, 2311.
[11] Y.-K. Chih, J.-C. Wang, R.-T. Yang, C.-C. Liu, Y.-C. Chang, Y.-S. Fu, W.-C. Lai, P. Chen, T.-C. Wen, Y.-C. Huang, C.-S. Tsao, T.-F. Guo, *Adv. Mater.* **2016**, *28*, 8687.
[12] Z.-K. Tan, R. S. Moghaddam, M. L. Lai, P. Docampo, R. Higler, F. Deschler, M. Price, A. Sadhanala, L. M. Pazos, D. Credgington, F. Hanusch, T. Bein, H. J. Snaith, R. H. Friend, *Nat. Nanotechnol.* **2014**, *9*, 1.
[13] H. Cho, S.-H. Jeong, M.-H. Park, Y.-H. Kim, C. Wolf, C.-L. Lee, J. H. Heo, A. Sadhanala, N. Myoung, S. Yoo, S. H. Im, R. H. Friend, T.-W. Lee, *Science* **2015**, *350*, 1222.
[14] L. Protesescu, S. Yakunin, M. I. Bodnarchuk, F. Krieg, R. Caputo, C. H. Hendon, R. X. Yang, A. Walsh, M. V. Kovalenko, *Nano Lett.* **2015**, *15*, 3692.
[15] S. Seth, N. Mondal, S. Patra, A. Samanta, *J. Phys. Chem. Lett.* **2016**, *7*, 266.
[16] A. Pan, B. He, X. Fan, Z. Liu, J. J. Urban, A. P. Alivisatos, L. He, Y. Liu, *ACS Nano* **2016**, *10*, 7943.
[17] K. Wu, G. Liang, Q. Shang, Y. Ren, D. Kong, T. Lian, *J. Am. Chem. Soc.* **2015**, *10*, 7943.
[18] Y. Kim, E. Yassitepe, O. Voznyy, R. Comin, G. Walters, X. Gong, P. Kanjanaboos, A. F. Nogueira, E. H. Sargent, *ACS Appl. Mater. Interfaces* **2015**, *7*, 25007.
[19] J. Song, J. Li, X. Li, L. Xu, Y. Dong, H. Zeng, *Adv. Mater.* **2015**, *27*, 7162.
[20] X. Zhang, B. Xu, J. Zhang, Y. Gao, Y. Zheng, K. Wang, X. W. Sun, *Adv. Funct. Mater.* **2016**, *26*, 4595.
[21] X. Zhang, H. Lin, H. Huang, C. Reckmeier, Y. Zhang, W. C. H. Choy, A. L. Rogach, *Nano Lett.* **2016**, *16*, 1415.
[22] G. Li, F. W. R. Rivarola, N. J. L. K. Davis, S. Bai, T. C. Jellicoe, F. de la Peña, S. Hou, C. Ducati, F. Gao, R. H. Friend, N. C. Greenham, Z. K. Tan, *Adv. Mater.* **2016**, *28*, 3528.
[23] Y. Ling, Y. Tian, X. Wang, J. C. Wang, J. M. Knox, F. Perez-Orive, Y. Du, L. Tan, K. Hanson, B. Ma, H. Gao, *Adv. Mater.* **2016**, *28*, 8983.
[24] J. Pan, L. N. Quan, Y. Zhao, W. Peng, B. Murali, S. P. Sarmah, M. Yuan, L. Sinatra, N. Alyami, J. Liu, E. Yassitepe, Z. Yang, O. Voznyy, R. Comin, M. N. Hedhili, O. F. Mohammed, Z. H. Lu, D. H. Kim, E. H. Sargent, O. M. Bakr, *Adv. Mater.* **2016**, *28*, 8718.
[25] J. Li, L. Xu, T. Wang, J. Song, J. Chen, J. Xue, Y. Dong, B. Cai, G. Shan, B. Han, H. Zeng, **2017**, *29*, 1603885.
[26] Q. A. Akkerman, V. D'Innocenzo, S. Accornero, A. Scarpellini, A. Petrozza, M. Prato, L. Manna, *J. Am. Chem. Soc.* **2015**, *137*, 10276.
[27] Y. Bekenstein, B. A. Koscher, S. W. Eaton, P. Yang, A. P. Alivisatos, *J. Am. Chem. Soc.* **2015**, *137*, 16008.
[28] X. Li, Y. Wu, S. Zhang, B. Cai, Y. Gu, J. Song, H. Zeng, *Adv. Funct. Mater.* **2016**, *26*, 2435.
[29] Q. A. Akkerman, S. G. Motti, A. R. Srimath Kandada, E. Mosconi, V. D'Innocenzo, G. Bertoni, S. Marras, B. A. Kamino, L. Miranda, F. De Angelis, A. Petrozza, M. Prato, L. Manna, *J. Am. Chem. Soc.* **2016**, *138*, 1010.
[30] M. A. Green, A. Ho-Baillie, H. J. Snaith, *Nat. Photonics* **2014**, *8*, 506.
[31] Y. Han, S. Meyer, Y. Dkhissi, K. Weber, J. M. Pringle, U. Bach, L. Spiccia, Y.-B. Cheng, *J. Mater. Chem. A* **2015**, *3*, 8139.
[32] J. Lee, Y. Chiang, *J. Mater. Chem.* **1999**, *9*, 3107.
[33] O. N. Yunakova, V. K. Miloslavsky, E. N. Kovalenko, V. V. Kovalenko, *Low Temp. Phys.* **2014**, *40*, 690.

© 2017 WILEY-VCH Verlag GmbH & Co. KGaA, Weinheim

Pursuant to the DOE Public Access Plan, this document represents the authors' peer-reviewed, accepted manuscript. The published version of the article is available from the relevant publisher.